

Studies on Corrosion Behaviors of Q235 Steel Coated by the Polypyrrole Films Doped with different dopants

Wenjie Zhou¹, Kongzhao Wu¹, Kun Zhang¹, ZheWang¹, ZhidingLiu¹, Shuchun Hu^{1,2,*}, Yong Fang^{2,*}, Chuan He²

¹ Key Laboratory of Advanced Technologies of Materials (Ministry of Education), School of Materials Science and Engineering, Southwest Jiaotong University, Chengdu 610031, China;

² Key Laboratory of Transportation Tunnel Engineering (Ministry of Education), Southwest Jiaotong University, Chengdu 610031, China.

*E-mail: schu@home.swjtu.edu.cn (Shuchun Hu), fy980220@swjtu.cn (Yong Fang)

Received: 27 October 2019 / Accepted: 17 January 2020 / Published: 10 February 2020

In this paper, polypyrrole (PPy) with different dopants was prepared on the surface of Q235 steel by a potentiostatic electrochemical deposition. The doping agents were using oxalic acid (OA), p-toluene sulfonic acid (p-TSA), sulfamic acid (SA), phytic acid (PA), and sodium dodecyl benzene sulfonate (SDBS). The FT-IR analysis of the products confirmed that the above dopants were incorporated into the PPy molecular chain. SEM observation and calculation results of the void ratio for the series of products indicated that the thickness of the PPy film with different dopants was equivalent, but the SDBS-PPy film layer had the smallest aggregate particle size and the highest film density. On this basis, the research results of the dynamic potential polarization curves and electrochemical impedance spectra for the bare Q235 and the prepared series of PPy/Q235 samples (OA-PPy/Q235, p-TSA-PPy/Q235, SA-PPy/Q235, PA-PPy/Q235 and SDBS-PPy/Q235) showed that the corrosion resistance of the series of PPy/Q235 samples had been significantly improved compared with the bare Q235. Furthermore, SDBS-PPy/Q235 showed the best anti-corrosion performance (with the maximum E_{corr} , the minimum I_{corr} and CR, as well as the maximum R_{ct} , R_{po} and R_{ox} and the minimum C_{dl} , Q_{po} and C_{ox}).

Keywords: potentiostatic; dopant; Q235; PPy; anti-corrosion performance

1. INTRODUCTION

Among the various conducting polymer materials, polypyrrole is widely used in various fields such as microbial fuel cells [1], absorbing materials [2], supercapacitors [3]. due to its raw materials availability, simple synthesis, and good stability, In recent years, many scholars have reported that polypyrrole can inhibit the corrosion of copper, magnesium, aluminium, stainless steel and other metals through good mechanical isolation, cathodic protection, corrosion inhibition and an ion release

mechanism; furthermore, the anti-corrosion effect is more prominent, which has attracted the much attention and research on the anti-corrosion performance and mechanism of PPy. Herrasti et al. [4] deposited a polypyrrole film with low porosity and uniformity on a copper surface by using a galvanostatic method, and found that the polypyrrole film exhibited excellent corrosion performance in a 3% NaCl solution. Cui X et al. [5] prepared a porous nanostructured PPy film layer on a magnesium electrode. The results showed that the PPy coating can effectively slow the corrosion of magnesium in physiological saline. I.L. Lehr et al. [6] prepared a molybdate-doped PPy film on the surface of an aluminium electrode, and the corrosion protection effect of the PPy film on the substrate was improved by regulating the electropolymerization process conditions. Hosseini MG et al. [7] deposited a polypyrrole phosphate (PPy-P) composite coating on the surface of ST12 mild carbon steel by cyclic voltammetry. The PPy-P composite coating provided better corrosion protection for mild steel than just a PPy coating. Jaouhari AE et al. [8] modified 304 stainless steel through an electrochemical deposition of a PPy film in an aqueous solution of sodium phthalate and sodium saccharin, respectively. The results showed that the PPy films had the same structural characteristics, and showed good corrosion resistance in a 3% NaCl solution.

In an early stage, an oxalic acid doped PPy film layer was prepared on the surface of Q235 steel by a potentiostatic method. The formation process and mechanism of the PPy film on the surface of Q235 steel were studied and reported; in the experimental study using a deposition potential range of 0.75-1.15 V, the PPy film layer had the best corrosion protection performance for Q235 steel when it was prepared at 0.95 V [9]. On the other hand, domestic and foreign scholars also widely recognize that doping PPy is an important way to explore anti-corrosion performance, in the field of PPy anti-corrosion performance research. Jiang L et al. [10] deposited different proton acid-doped PPy film layers on 304 stainless steel. It was found that a phosphoric acid-doped PPy film layer had a smooth and compact surface, showing better corrosion resistance. Wang Gui Xiang et al. [11] demonstrated that a PPy-MoO₄²⁻ coating had better corrosion resistance and lower surface resistance compared with that of pure PPy; the PPy and PPy-MoO₄²⁻ films were produced on an AZ31 magnesium alloy by using cyclic voltammetry in a sodium salicylate solution. Castagno et al. [12] polymerized sodium dodecylbenzene sulfonate-doped PPy film on an aluminium alloy 1100, which showed better corrosive resistance in 0.05 mol L⁻¹ NaCl and 0.05 mol L⁻¹ HCl solution. Combined with the above two aspects, in this paper, polypyrrole (PPy) films with different dopants were prepared on the surface of Q235 steel by potentiostatic electrochemical deposition (deposition potential 0.95 V). We used oxalic acid (OA), p-toluenesulfonic acid (p-TSA), sulfamic acid (SA), phytic acid (PA), and sodium dodecyl benzene sulfonate (SDBS) as dopants. A comparative study of the corrosion protection performance of the series of products on Q235 steel, was conducted to explore which type of dopant is most beneficial for improving PPy corrosion resistance.

2. EXPERIMENTAL PROCEDURES

2.1 Reagents and materials

All chemicals such as pyrrole monomer, oxalic acid (C₂H₂O₄·2H₂O), sodium dodecyl benzene sulfonate (C₁₈H₂₉NaO₃S), toluene-p-sulfonic acid (C₇H₈O₃S), sulfamic acid (NH₂SO₃H), phytic acid (C₆H₁₈O₂₄P₆), sodium chloride (NaCl), and ethanol were analytically pure and used as received. The

distilled water was made by the laboratory. Silicon resin for sealing the working electrodes was commercially available. The chemical compositions of Q235 steel are listed in Table 1.

Table 1. Chemical composition of Q235 steel (wt.%)

C	Si	Mn	P	S	Fe
0.16	0.30	0.53	<0.045	<0.055	balance

2.2 Sample preparation

The preparation of the working electrode is referred to in reference [9].

In this paper, the PPy film layer is deposited on the surface of the Q235 substrate by a previously reported method from the research group. Taking OA doping as an example, first, the solution in the electrolytic cell was prepared from distilled water, 0.1 M pyrrole and 0.1 M oxalic acid. Then, via a CHI660E electrochemical workstation, a polypyrrole-modified Q235 sample (denoted as OA-PPy-Q235) was obtained. The temperature of the preparation process was 3 °C (by an ice-water mixing bath), and the magnetic stirring speed was 600 r/min. The PPy prepared with different dopants (p-TSA, SA, PA, SDBS) were obtained by setting the potentiostatic mode in the above process to 0.95 V and denoted as PTSA-PPy/Q235, SA-PPy/Q235, PA-PPy/Q235 and SDBS-PPy/Q235, respectively.

2.3 Sample characterization

The infrared absorption spectrum of the prepared PPy-Q235 thin film was measured with a Thermo Fisher Nicolet 6700 infrared spectrometer. KBr tablets were adopted, and the wave number ranged from 400 to 4000 cm^{-1} . The deposited film morphologies of the PPy-Q235 samples were observed with a Quanta 200 scanning electron microscope, using an acceleration voltage of 20.0 kV. The thickness of the film was measured by a Qnix4500 German coating thickness gauge.

2.4 Electrochemical test

Corrosion tests on bare Q235 and PPy-Q235 samples were performed on a CHI660E electrochemical workstation, at room temperature, and in a 3.5% NaCl solution. A three-electrolysis cell with a Luggin Capillary was used in the test, with a 1 cm × 1 cm platinum plate, a saturated calomel electrode (SCE) and a Q235 substrate as the counter electrode, the reference electrode and the working electrode, respectively. The open-circuit potential (E_{ocp}) was used as the initial potential in AC impedance spectroscopy, and a 10 mV sinusoidal wave signal was applied. The frequency range of the measurements was from 10 mHz to 100 kHz. The potential range of the potentiodynamic polarization curve was approximately 250 mV of the open circuit potential, that is, $E_{\text{ocp}}-250 \text{ mV} \sim E_{\text{ocp}}+250 \text{ mV}$, and the scan rate was 1 mV s^{-1} .

3. RESULTS AND DISCUSSION

3.1 Scanning electron microscopy

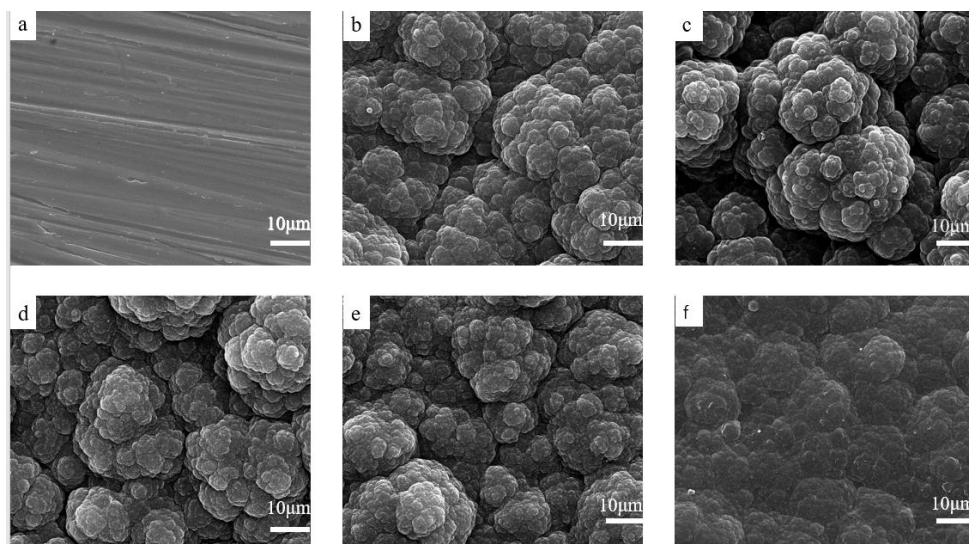


Figure 1. SEM of the synthesized films at constant potential in a magnetically stirred ice bath: (a) bare Q235, (b) OA-PPy/Q235, (c) PTSA-PPy/Q235, (d) SA-PPy/Q235, (e) PA-PPy/Q235, and (f) SDBS-PPy/Q235.

Fig. 1 shows the surface morphology of the bare Q235 and SEM images of the deposited films of the PPy-Q235 samples prepared with different dopants. Fig. 1(a) shows the surface of the bare Q235 is smooth and flat, while the electrochemically deposited PPy films of the PPy-Q235 samples, show a typical cauliflower-like microscopic morphology, as shown in Fig. 1(b-f). Therefore, the polymerization capacity of the α -position and the β -position in the pyrrole monomer is equivalent, so the PPy formed in the polymerization grows in three dimensions and eventually forms a cauliflower-like microstructure [13]. The thicknesses of the PPy films of the PPy-Q235 samples were all measured to be 40 μm . Moreover, the average diameters of the OA-PPy/Q235, PTSA-PPy/Q235, SA-PPy/Q235, PA-PPy/Q235, SDBS-PPy/Q235 product particles, as shown in Fig. 1 (b-f), were measured by Nano Measurer 1.2.5 software and were 0.69 μm , 0.63 μm , 0.71 μm , 0.58 μm and 0.48 μm , respectively. The particle size is inversely proportional to the density of the film layer, and the SDBS-doped PPy particles have the smallest size; thus, the film is denser and flatter compared with those of the other four samples.

3.2 FT-IR analysis of the synthetic films

Figure 2 (a-e) corresponds to the infrared spectrum of the polypyrrole layer with five different dopants, including OA, PTSA, SA, PA, and SDBS. Absorption peaks appear in the five samples at 3421 cm^{-1} and 1540 cm^{-1} . Among them, 3421 cm^{-1} is attributed to the N-H stretching vibration [14], and 1540 cm^{-1} is attributed to the pyrrole ring C=C stretching vibration [15]. Furthermore, peaks at 2854 cm^{-1} and 2925 cm^{-1} correspond to the symmetric and asymmetric stretching vibrations of $-\text{CH}_2$, respectively [16], and 1400 cm^{-1} is attributed to the C-C stretching vibrations on the pyrrole ring [17].

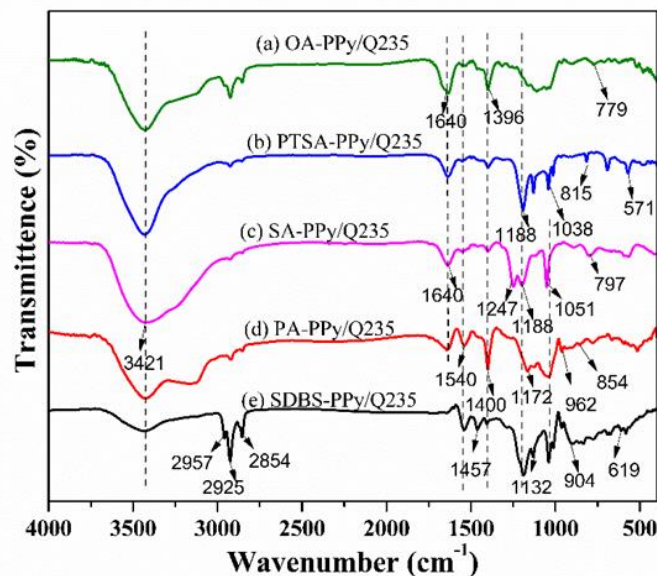


Figure 2. FT-IR spectra of the deposition films under magnetic stirring in an ice bath: (a) OA-PPy/Q235, (b) PTSA-PPy/Q235, (c) SA-PPy/Q235, (d) PA-PPy/Q235, and (e) SDBS-PPy/Q235.

This outcome shows that the deposited film layers are all polypyrrole. In addition, in Fig. 2(a), peaks at 1396 cm^{-1} and 1640 cm^{-1} correspond to the symmetric and asymmetric vibrational absorption of COO groups [18], so $\text{C}_2\text{O}_4^{2-}$ was doped into the PPy molecular chain. In Fig. 2(b), the absorption peak at 1188 cm^{-1} is attributed to the sulfonate anion $-\text{SO}_3\text{H}$, and the S-phenyl and S-O absorption peaks are at 1063 cm^{-1} and 1188 cm^{-1} , respectively. The peak near 1640 cm^{-1} is related to the O-H bending vibration [19], and the absorption peak at 815 cm^{-1} is the C-H out-of-plane bending vibration (1,4 substitution) on the benzene ring. In Fig. 2(c), 1247 cm^{-1} is derived from the N-H bending vibration, and the absorption peak at 1188 cm^{-1} is related to $-\text{SO}_3\text{H}$. The peak near 1640 cm^{-1} corresponds to the O-H bending vibration. In Fig. 2(d), the peaks at 1172 cm^{-1} , 962 cm^{-1} , and 854 cm^{-1} are characteristic absorption peaks of phytic acid [20]. The peaks at 962 cm^{-1} and 854 cm^{-1} are attributed to the P-O-C stretching vibration, the peak at 1172 cm^{-1} is derived from the P=O stretching vibration, the peak at 1038 cm^{-1} is derived from the stretching vibration of P-OH, and the peak near 1640 cm^{-1} is attributed to the related O-H bending vibration. In Fig. 2(e), the peak at 2957 cm^{-1} is the C-H stretching vibration in $-\text{CH}_3$, and the absorption peaks at 1188 cm^{-1} and 1038 cm^{-1} are related to the sulfonate anion $-\text{SO}_3\text{H}$ [21,22]. The peaks at 1132 cm^{-1} and 610 cm^{-1} are derived from the $-\text{S}=\text{O}$ stretching vibration, thereby indicating that the SDBS was doped into the PPy. Based on the above analysis, the five different dopants, OA, PTSA, SA, PA and SDBS, were successively doped into the PPy film layer.

3.3 Anti-corrosion property of the PPy-Q235 samples

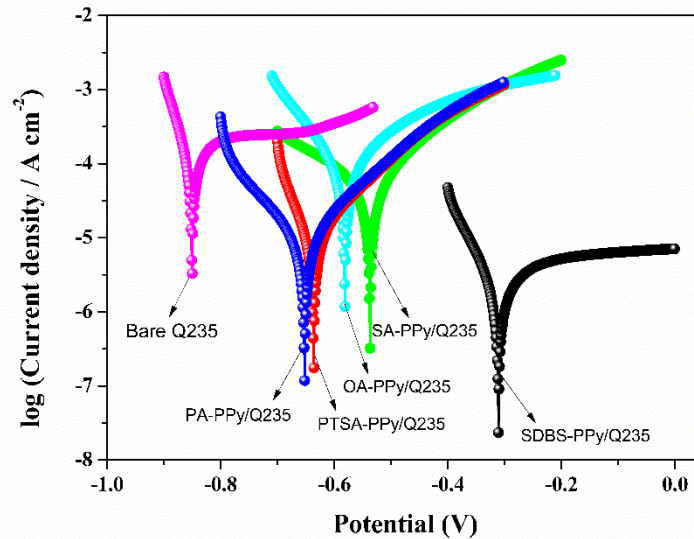


Figure 3. Tafel polarization curves of the bare Q235 and the PPy-Q235 samples (after immersion in the 3.5% NaCl solution in 30 min).

Table 2. E_{corr} , I_{corr} , R_p and CR values of the bare Q235 and PPy-Q235 samples.

Samples	E_{corr}/V	$I_{corr}/\mu A/cm^2$	$b_a (V/dec)$	$-b_c (V/dec)$	$R_p (\Omega/cm^2)$	Corrosion rate (mm/y)
Bare Q235	-0.850	105.90	0.144	0.039	126	1.234
OA-PPy/Q235	-0.581	56.78	0.145	0.102	459	0.662
PTSA-PPy/Q235	-0.625	31.32	0.139	0.675	1600	0.465
SA-PPy/Q235	-0.540	69.18	0.135	0.041	196	0.806
PA-PPy/Q235	-0.650	10.23	0.143	0.117	2433	0.119
SDBS-PPy/Q235	-0.311	4.34	0.096	0.058	9620	0.050

Fig. 3 shows the Tafel polarization curves of the bare Q235 and the polypyrrole films prepared with various dopants, after being immersed in the 3.5% NaCl solution for 30 min. Based on the polarization curves of each sample, the corrosion potential E_{corr} and corrosion current I_{corr} can be calculated by the Tafel extrapolation method. On this basis, the corrosion rate (CR) of each sample can be calculated by Eq. (1) [23]:

$$CR = \frac{[3272I_{corr}(EW)]}{Ad} \tag{1}$$

where CR is the corrosion rate in millimetres per year, I_{corr} is the corrosion current in amperes per square centimetre, EW is the equivalent in grams (EW of Q235 is 28g [24]), A is the surface area of the sample (in square centimetres), and d is the density of the sample (in grams per cubic centimetre),

which for Q235 is 7.86 g/cm^3 [9]. The E_{corr} , I_{corr} and CR values for the bare Q235 and PPy-Q235 samples are listed in Table 2.

In addition, the polarization resistance R_p can be calculated by Eq. (2)[25]:

$$R_p = b_a b_c / 2.3j_{corr} (b_a + b_c) \quad (2)$$

where j_{corr} (also labelled as I_{corr}) is the corrosion current density listed in Table 2, and b_a and b_c are the anode and cathode Tafel slopes obtained from the potentiodynamic polarization curves, respectively. The R_p values of the bare Q235 and PPy-Q235 samples are calculated, according to Eq. (2), and listed in Table 2.

As can be learned from Table 2, the E_{corr} of the bare Q235 is -0.850 V , and the corrosion potential of the other five samples is between -0.650 V ~ -0.311 V , which indicates that the electrochemical deposition of polypyrrole film can significantly improve the self-corrosion potential of Q235 steel. In addition, the corrosion current of bare Q235 is $105.90 \mu\text{A/cm}^2$, and the calculated annual corrosion rate is 1.234 mm/y , while the other doped samples show a significant reduction in corrosion current. Table 2 shows that the corrosion current of SDBS-PPy/Q235 is the smallest, with a value of $4.34 \mu\text{A/cm}^2$, meaning it shows the best corrosion resistance. The CR value of SDBS-PPy/Q235 is the lowest CR, which is approximately $1/25$ the value for the bare Q235, further indicating that SDBS-PPy has the best anti-corrosion performance.

Moreover, the porosity (P) of the deposited films of PPy-Q235 samples can be calculated using Eq. (3) [26]:

$$P = \frac{R_{ps}}{R_{pc}} \times 10^{-\left(\frac{|\Delta E_{corr}|}{b_a}\right)} \quad (3)$$

where P is the total porosity of the PPy-Q235 deposited film, R_{pc} is the measured polarization resistance of PPy-Q235, R_{ps} is the polarization resistance of the bare Q235, ΔE_{corr} is the difference between the corrosion potentials of the PPy-Q235 and bare Q235, and b_a is the anodic Tafel slope for the bare Q235. With Eq. (3), the film porosities of the OA-PPy/Q235, PTSA-PPy/Q235, SA-PPy/Q235, PA-PPy/Q235, SDBS-PPy/Q235 were calculated to be 3.7×10^{-3} , 2.2×10^{-3} , 4.5×10^{-3} , 2.1×10^{-3} and 5.5×10^{-6} , respectively, these porosities were consistent with the analysis and calculation results from the SEM analysis. The larger the diameter of the sample is, the greater the porosity, and the corrosion rate is inversely proportional to the porosity, which is related to the mechanical isolation mechanism of PPy.

Fig. 4 shows the Nyquist and Bode plots of the PPy-Q235 samples in the 3.5% NaCl solution. Among these figures, Fig. 4(a) shows the Nyquist plots (the insert diagram shows the local amplification), Fig. 4(b) is the $\log |Z|$ vs $\log f$ plots, and Fig. 4(c) shows the phase angle vs $\log f$ plots. EIS is a method that can effectively study the characteristics of interfacial electrochemical reactions [27]. The electrochemical activity strength and impedance of the test electrode can be reflected by measuring the diameter of the EIS curve. The larger EIS curve diameters, indicate that it is more difficult to transfer the surface charge of the electrode and thus, has a larger charge transfer resistance. Fig. 4(a) shows that in the low-frequency linear region, they all demonstrate Warburg impedance, indicating that the diffusion process is an important step in the electrode process, and that the redox reaction takes place in the film [9].

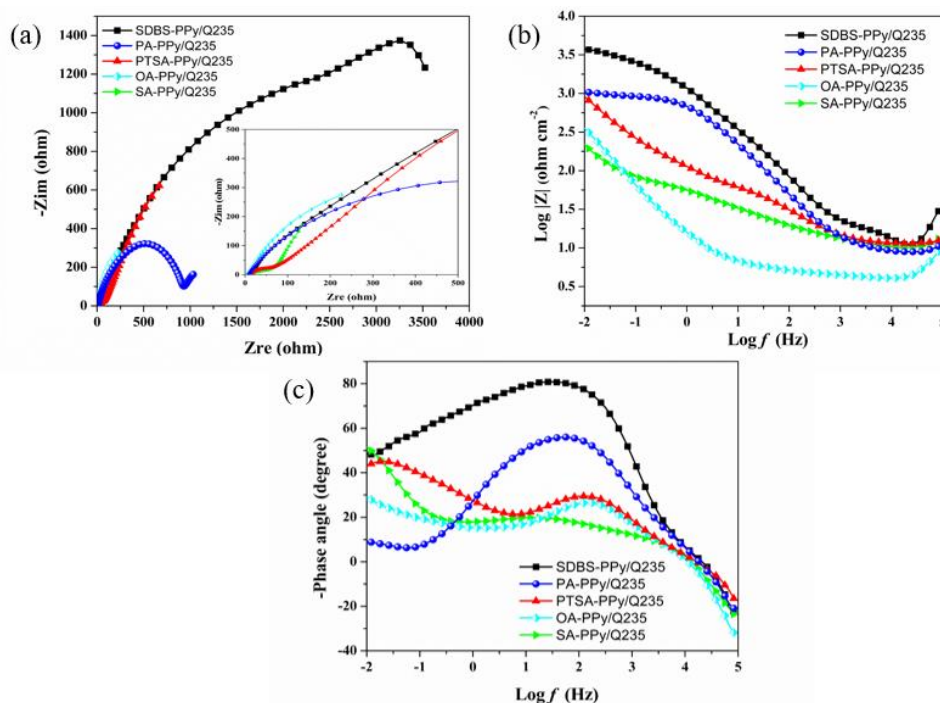


Figure 4. Nyquist and Bode plots of the prepared PPy-Q235 samples.

It is widely recognized that if the sample has a large impedance modulus in the low-frequency region and a high phase angle in the high-frequency region, then the corrosion performance is better [28]. It is obvious, as shown in Fig.4 (b-c), that SDBS-PPy/Q235 has the largest modulus in the low-frequency domain and the highest phase angle in the high-frequency domain; this outcome shows that SDBS-PPy/Q235 has the best anti-corrosion performance among all the PPy-Q235 samples. Outside of SDBS-PPy/Q235, the anti-corrosion performance is in the following order: PA-PPy/Q235, PTSA-PPy/Q235, OA-PPy/Q235, and SA-PPy/Q235, which is consistent with the analysis results of the Tafel polarization curves.

In addition, the corresponding equivalent circuit diagram was obtained and is shown in Fig. 5. In the Fig. 5, L is the equivalent inductance, R_{sol} is the resistance of the electrolyte solution, R_{ct} is the charge transfer resistance, R_{po} is PPy coating pore resistance, R_{ox} is the resistance of oxide films, C_{dl} is the double layer capacitance at interface, C_{ox} is the capacitance of the oxide film, Q_{po} is the capacitance of the polypyrrole film, and W is the Warburg impedance. Table 3 provides the electrochemical parameters fitted by ZsimpWin 3.10 for the equivalent circuit models. It is generally believed that the parameters of the equivalent circuit diagram are related to the corrosion behaviour of the samples. Generally, samples with high R values (R_{ct} , R_{po} and R_{ox}) and low C values (C_{dl} , Q_{po} and C_{ox}) demonstrate superior corrosion resistance. As seen from Table 3, R_{ct} , R_{po} and R_{ox} of SDBS-PPy/Q235 (the values are 5.441, 233, 0.1702 Ωcm^{-2} , respectively) are higher than the other four samples, and its C_{dl} , Q_{po} and C_{ox} (the values are 8.561×10^{-6} F/ cm^2 , 7.514×10^{-6} S cm^{-2} , 1.41×10^{-6} F/ cm^2 , respectively) are lower than the other four. The above results indicate that SDBS-PPy/Q235 has the best corrosion resistance.

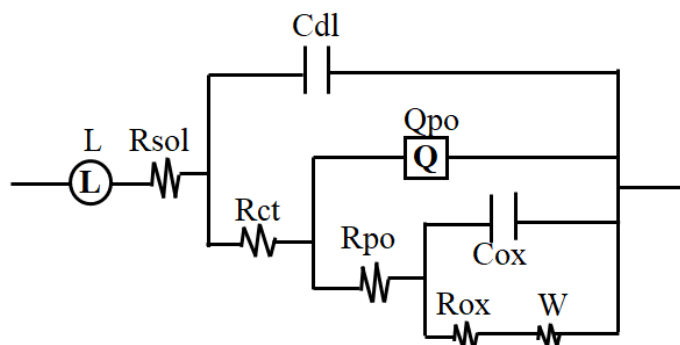


Figure 5. Equivalent circuit for fitting the impedance diagram of PPy-Q235.

Table 3. EIS parameters fitted by the equivalent circuits proposed in Fig. 5.

Samples	L	R_{sol} (ohm/cm ²)	C_{dl} (F/cm ²)	R_{ct} (ohm/cm ²)	Q_{po} (S sec ⁿ cm ⁻²)	n	R_{po} (ohm/cm ²)	C_{ox} (F/cm ²)	R_{ox} (ohm/cm ²)	W (S sec ⁵ cm ⁻²)
OA-PPy/Q235	1.24×10^{-5}	4.287	4.08×10^{-4}	1.105	0.0176	0.7338	53.6	4.07×10^{-3}	1213	1.94×10^{-9}
PTSA-PPy/Q235	6.62×10^{-6}	11.48	1.53×10^{-5}	2.241	9.84×10^{-4}	0.5487	86.37	1.03×10^{-3}	9.68×10^{-3}	4.04×10^{-3}
SA-PPy/Q235	1.04×10^{-5}	10.43	2.06×10^{-5}	4.409	1.96×10^{-3}	0.6381	0.0153	2.27×10^{-10}	33.52	0.0222
PA-PPy/Q235	7.75×10^{-6}	8.935	9.72×10^{-6}	4.164	2.09×10^{-4}	0.6832	992.8	0.0902	444.5	0.0988
SDBS-PPy/Q235	7.68×10^{-6}	8.873	8.56×10^{-6}	5.441	7.51×10^{-6}	0.965	233	1.41×10^{-6}	0.1702	3.18×10^{-5}

4. CONCLUSIONS

Polypyrrole (PPy) films were prepared on the surface of Q235 steel by a potentiostatic method (deposition potential: 0.95 V), using OA, p-TSA, SA, PA, SDBS as doping agents. An approximately thickness of 40 μm is shown for the series of film products. Among the prepared series of PPy films, the SDBS-PPy film has the smallest aggregate particle size and the highest film density. The results of the dynamic potential polarization curves and electrochemical impedance spectroscopy of the bare Q235 and series of PPy/Q235 products show that the corrosion resistance of the series of PPy/Q235 samples has been significantly improved compared with that of the bare Q235. Moreover, SDBS-PPy/Q235 shows the best anti-corrosion performance (with the maximum E_{corr} , the minimum I_{corr} and CR, as well as the maximum R_{ct} , R_{po} , R_{ox} and the minimum C_{dl} , Q_{po} , C_{ox}), which indicates that SDBS as a doping agent is the most beneficial for improving the corrosion protection of PPy on Q235 steel.

ACKNOWLEDGMENTS

We express our great thanks to the financial support from the National Natural Science Foundation (Grant No. 51609204) and the Key Program of National Natural Science Foundation of China (Coal joint fund) (Grant No. U1361210).

References

1. P. Mishra, R. Jain, *Int. J. Hydrogen Energy*, 41 (2016) 47.
2. S. Hu, Y. Zhou and L. Zhang, *J. Mater. Sci.*, 53.4 (2018) 3016-3026.
3. X. Lu, Z. Shen and Z. Zhang, *ACS Appl. Mater. Interfaces*, 10.4 (2018) 4041-4049.

4. P. Herrasti, A.I. Del Rio and J. Recio, *Electrochim. Acta*, 52.23 (2007) 6496-6501.
5. X. Cui, X. Huang and Y. He, *Synth. Met.*, 195 (2014) 97-101.
6. IL. Lehr, S.B. Saidman, *Electrochim. Acta*, 51.16 (2006) 3249-3255.
7. M.G. Hosseini, M. Sabouri and T. Shahrabi, *Prog. Org. Coat.*, 60.3 (2007) 178-185.
8. A.E. Jaouhari, S.B. Jadi and Z. Aouzal, *Polym. Test.*, 67 (2018) 302-308.
9. L. Zhang, S. Liu, and H. Han. *Surf. Coat. Technol.*, 341 (2018) 95-102.
10. L Jiang, H. Ma and J. Zhang, *MATEC Web of Conferences*, 109 (2017) 03007.
11. G.X. Wang, N.N. Cao and X.H. Zhang, *Rare Metal Materials and Engineering*, 46.6 (2017) 1480-1485.
12. Castagno, R.L. Kátia, V. Dalmoro and S.A. Denise, *Materials Chemistry & Physics*, 130.1-2 (2011) 721-726.
13. J. Joo, J.K. Lee and J.S. Baeck, *Synth. Met.*, 117.1-3 (2001) 45-51.
14. X.F. Lu, H. Mao and W.J. Zhang, *Polym. Compos.*, 30.6 (2009) 847-854.
15. X.H. Zhang, R.G. Xie, and L.T Sun, *J. Phys. Chem. B*, 37.15 (2006) 2-4.
16. P.H. Aoki, D. Volpati, W. Caetano and C.J. Constantino, *Vib. Spectrosc.*, 54 (2010) 93-102.
17. M. Trueba, S.P. Trasatti, *Prog. Org. Coat.*, 66.3 (2009) 254-264.
18. G. Matela, R. Aman, C. Sharma and S. Chaudhary, *Adv. Chem. Sci.*, 1 (2013) 157-163.
19. Y.F. Li, Y. Ling and H. Zhen, *Chinese Journal of Inorganic Chemistry*, 24.1 (2008) 117-123.
20. N. Wang, H. Dai and D. Wang, *Mater. Sci. Eng., C*, 76 (2017) 139-143.
21. R.M. Silverstein, F.X. Webster and D.J. Kiemle, *Spectrometric Identification of Organic Compounds*, 7th ed, John Wiley&Sons, Inc., Hoboken 2 (2005) 106.
22. F. Li, B. Yu, C. Jia, *Langmuir*, 26.14 (2010): 12314-12320.
23. Operating Manual for CMS 100 Corrosion Measurement System, Gamry Instruments, Inc., PA, USA.
24. W: Pierre Larousse, *Grand dictionnaire universel du XIXe siècle*", vol. I, (1866) 871.
25. A. Omrani, H. Rostami and R. Minaee, *Prog. Org. Coat.*, 90 (2016) 331-338.
26. J. Creus, H. Mazille, H. Idrissi, *Surf. Coat. Technol.*, 130 (2000) 224-232.
27. S. Panero, P. Prospero and B. Scrosati, *Electrochim. Acta*, 32.10 (1987) 1461-1464.
28. L.K. Wu, X.F. Zhang and J. M. Hu, *Corros. Sci.*, 85 (2014) 482-487.